

Defects in Lamellar Diblock Copolymers: Chevron- and Omega-shaped Tilt Boundaries

Yoav Tsori and David Andelman

*School of Physics and Astronomy, Raymond and Beverly Sackler Faculty of Exact Sciences
Tel Aviv University, 69978 Ramat Aviv, Israel*

Michael Schick

*Department of Physics, Box 351560
University of Washington, Seattle, WA 98195-1560
(May 24, 1999)*

The lamellar phase in diblock copolymer systems appears as a result of a competition between molecular and entropic forces which select a preferred periodicity of the lamellae. Grain boundaries are formed when two grains of different orientations meet. We investigate the case where the lamellae meet symmetrically with respect to the interface. The form of the interface strongly depends on the angle, θ , between the normals of the grains. When this angle is small, the lamellae transform smoothly from one orientation to the other, creating the chevron morphology. As θ increases, a gradual transition is observed to an omega morphology characterized by a protrusion of the lamellae along the interface between the two phases. We present a theoretical approach to find these tilt boundaries in two-dimensional systems, based on a Ginzburg-Landau expansion of the free energy which describes the appearance of lamellae. Close to the tips at which lamellae from different grains meet, these lamellae are distorted. To find this distortion for small angles, we use a phase variation ansatz in which one assumes that the wave vector of the bulk lamellar phase depends on the distance from the interface. Minimization of the free energy gives an expression for the order parameter $\phi(x, y)$. The results describe the chevron morphology very well. For larger angles, a different approach is used. We linearize ϕ around its bulk value ϕ_L and expand the free energy to second order in their difference. Minimization of the free energy results in a linear fourth order differential equation for the distortion field, with proper constraints, similar to the Mathieu equation. concentration profile and line tension obtained agree qualitatively with transmission electron microscope experiments, and with full numerical solution of the same problem.

I. INTRODUCTION

The lamellar phase is one of the possible phases with spatial modulations that can be found in a wide variety of physical and chemical systems. These include diblock copolymer melts, mixtures of diblock and homopolymers, aqueous solutions of lipids or surfactants, Langmuir monolayers, and magnetic garnet films [1]. Modulated phases are the result of a competition between opposing forces, one of which prefers ordering characterized by a non-zero wavenumber, while the other prefers a homogeneous (disordered) state. Below we shall employ the language appropriate to block-copolymers, but our work applies equally to the other systems.

We consider diblock copolymer melts in which the two polymer blocks are incompatible. This incompatibility is characterized by a positive Flory parameter χ . Because of the covalent chemical bond between the A and B blocks, the system cannot undergo a true macrophase separation. Instead it undergoes a *microphase separation* characterized by A- and B-rich domains of a finite size. Various modulated phases such as lamellar, hexagonal, and cubic are observed [2–7] depending upon the χ parameter as well as on the relative lengths of A and B blocks. In most cases, the χ parameter depends inversely on the temperature. Hence, the lamellar and other modulated phases will not be stable at high temperatures and the polymer melt will be in a disordered state.

The equilibrium behavior of diblock copolymers in the bulk is by now well understood [5–7]. Single domain bulk phases, however, are rarely observed in experiments because it is extremely difficult to completely anneal defects. In most cases, due to very slow dynamics and energy barriers, the microstructural ordering is limited to finite-size domains (or grains) separated by grain boundaries. These defects are very common to block copolymer systems and are readily observed in experiments [3,4].

Because these domain boundaries and defects are so abundant in polymer melts, it is of interest to study their energetics and other characteristics. In this paper we concentrate on the relatively simple situation of domain boundaries in lamellar phases in which there is no twist between the two grains, only a tilt, as is shown schematically in Fig. 1a. The system is translationally invariant along the z -direction and can be described by its x - y cross-section only, reducing it to an effective two dimensional system. As can be seen in Fig. 1a, the distance between lamellae along the grain boundary d_x is larger than d , the lamellae spacing in bulk, by a factor of $1/[\cos(\theta/2)]$. This causes an increase in the local free energy density related to the grain boundary. The experiments of Gido and Thomas [3] and Hashimoto and coworkers [4] show that the response of the system to this increase in free energy depends strongly on the tilt angle θ between the grains. Chevron morphology occurs when the angle is small. In such a situation, lamellae transform smoothly from one orientation to the other, creating V-shaped rounded tips which reduce the interfacial area between lamellae at the expense of introducing a curvature energy. This situation is shown schematically in Fig. 1b. A gradual transition to an omega-shaped tip is observed when θ is increased. This morphology is characterized by protrusions of the lamellae along the interface between the two phases. The protrusions can be understood as a different attempt of the system to reduce the cost of the boundary, while still complying with the geometrical constraints. Essentially the system tries to create a lamella similar to those in the bulk but which is aligned along the interface itself.

The basic phenomenology of these grain boundaries was presented by Gido and Thomas [3]. Netz, Andelman, and Schick [2] then considered the phenomenon employing a Landau free energy which was minimized numerically, and obtained both the chevron and omega morphologies. Matsen [9] considered the block-copolymer system explicitly and employed self-consistent field theory. Not only did this produce the chevron and omega morphologies, but also a symmetry-broken omega in which the response (and shape) of lamellae composed of one of the blocks differs from that of the other. The general configuration is omega-like. Such symmetry broken boundaries were indeed observed by Gido and Thomas [3].

In Sec. II we adopt the Landau free energy functional employed earlier [2]. The advantages to using this functional are its simplicity and generality, while retaining the essential ingredients that capture the behavior of the system. In contrast to the complete minimization of the free energy functional which requires a numerical calculation, we shall employ here a simple ansatz for the form of the grain boundary in order to obtain analytic results. Recently, similar methods were employed to obtain analytically the interface between the lamellar and disordered phases of diblock copolymers [8]. Our motivation is to demonstrate that the essence of these interesting morphologies does not depend on strong segregation conditions or a large number of Fourier components, and so should be observable in all systems with modulated phases.

The chevron structure is obtained by using the bulk lamellar phase solution with a constant amplitude, but with varying wavevector. Minimizing the free energy subject to the proper geometrical constraints, we find an equation for the wavevector. This is done in Sec. III. Beyond the chevron regime (large inter-domain angles), this approach will not be adequate, because the amplitude of modulations will have to vary as well. To this end we expand $\phi(x, y)$ around the two bulk lamellar phases, giving rise to an equation for a small distortion field. Close to the interface, the sharp tips of the lamellar phase (see Fig. 1a) are smoothed-out and the protrusion characteristic of the omega morphology appears. Far away from the interface, the disturbance vanishes and the bulk lamellar phase is recovered,

as is shown in Sec. IV. In Sec. V we discuss some features of our method, the analogy to, and the differences from the Schrödinger equation for electrons in a one-dimensional periodic potential (known also as the Mathieu equation). In Sec. VI we report our results, and discuss them in Sec. VII.

II. THE MODEL

An order parameter $\phi(x, y) = (\phi_A - \phi_B) / (\phi_A + \phi_B)$ is used to describe the deviation of the (dimensionless) concentration of the A and B monomers from the symmetric 1:1 composition. We employ the following Ginzburg-Landau dimensionless free energy density:

$$F = -\frac{1}{2}\chi\phi^2 + \frac{1-\phi}{2}\ln\frac{1-\phi}{2} + \frac{1+\phi}{2}\ln\frac{1+\phi}{2} - \frac{1}{2}(\nabla\phi)^2 + \frac{1}{2}(\nabla^2\phi)^2 \quad (1)$$

The first term, proportional to χ , represents the repulsive interaction between the two incompatible polymer blocks. It induces the system towards macro-phase separation, with the system being divided between an A-rich and a B-rich coexisting phases, both characterized by a non-zero order parameter, $\phi \neq 0$. The next two terms are the usual ideal entropy of mixing contributions, which favor a $\phi = 0$ disordered state. The last two terms arise from short range interactions in the blocks. That the gradient squared term is negative means it induces the system to a modulated phase, while the Laplacian squared term ensures that these modulations are not too large. This type of free energy functional (and some variants of it) has been successfully used to describe the bulk phase of diblock copolymers [5,6], amphiphilic systems [10], Langmuir films [11] and magnetic sheets [12].

For the weak segregation limit, i.e. $|\phi| \ll 1$, the free energy density can be expanded to fourth order in ϕ yielding

$$F = \frac{1}{2}(1-\chi)\phi^2 + \frac{1}{12}\phi^4 - \frac{1}{2}(\nabla\phi)^2 + \frac{1}{2}(\nabla^2\phi)^2 \quad (2)$$

Assuming an infinite system that is non-uniform only along the x direction, one can minimize the free energy to obtain the solution describing the lamellar phase ϕ_L having a one-dimensional symmetry:

$$\phi_L = \phi_0 + \phi_q \cos(qx) \quad (3)$$

with ϕ_0 the average concentration, $q = 1/\sqrt{2}$ the optimal wavevector, and $\phi_q = 2\sqrt{\chi - \phi_0^2 - 3/4}$ the amplitude of the variations [8]. It can be shown [5–7] that this lamellar phase is the thermodynamical stable phase in some range of the system parameters: ϕ_0 and χ .

A few remarks are now in order. First, as was mentioned in the introduction, the free energy (2) can have other non-lamellar modulated solution [2,13]. We will not consider them in this paper since our aim is to study defects *inside* lamellar phases. Second, the validity of a single optimal mode can be justified in the weak segregation limit (i.e., being close to a critical point). Far from the critical point higher harmonics are needed to describe the optimal lamellar phase [2]. Third, we obtain a wavenumber q which is a constant number, independent of other system parameters. This is a result of the simple choice of the prefactors in the gradient squared and Laplacian squared terms in Eq. (2), and should be regarded as an over-simplification of real physical systems.

We now turn to the tilt-boundary problem, where two lamellar domains, both lying parallel to the x - y plane, meet with an angle θ between their normals. (See Fig. 1a.) The x -axis is along the line interface between the two lamellar domains. The y -axis is perpendicular to it. In these variables the lamellae in the two grains are described by

$$\phi_L = \phi_0 + \phi_q \cos(q_x x \pm q_y y) \quad (4)$$

where $q_x \equiv q \cos(\theta/2)$ and $q_y \equiv q \sin(\theta/2)$ are the components of the optimal wavevector, \vec{q} . Their inverses provide characteristic length scales in the x and y directions, respectively. The $y < 0$ half plane is a reflection through the x axis of the $y > 0$ half plane, so it is sufficient to consider only the upper half plane, $y > 0$. The system is periodic along the x axis, with wavelength $d_x = 2\pi/q_x = 2\pi/[q \cos(\theta/2)]$.

III. DESCRIPTION OF THE CHEVRONS

For small tilt angles, the lamellae transform smoothly from one orientation to the other, showing the chevron morphology. We will assume that for small enough tilt angles, the only change of the functional form of the order parameter is through the wavevector [14,15]. The aim of this section is to show that, in the chevron regime, the

behavior of the system close to the interface is, in essence, quite similar to that far from the interface. The diagonal lines in Fig. 1a show each bulk lamellar phase in its respective half-plane, and the sharp tips which result from their intersection. These sharp tips will be smoothed out in the chevron morphology, Fig. 1b.

We use the following ansatz for $\phi(x, y)$:

$$\phi(x, y) = \phi_0 + \phi_q \cos[q_x x + q_x u(y)] \quad (5)$$

The local direction and magnitude of the wavevector depends on the distance y from the x -axis. Far away from the interface, the lamellae must return to their bulk values, implying

$$\lim_{y \rightarrow \pm\infty} u(y) = \mp (q_y/q_x) y = \mp \tan(\theta/2) y \quad (6)$$

$$\lim_{y \rightarrow \pm 0} u(y) = 0 \quad (7)$$

$$\lim_{y \rightarrow \pm 0} u'(y) = \mp \tan(\theta/2) \quad (8)$$

Symmetry with respect to inversion across the x -axis means that

$$\left. \frac{\partial \phi}{\partial y} \right|_{y=0} = -\phi_q q_x u'(0) \sin(q_x x) = 0 \quad (9)$$

which implies

$$u'(0) = 0 \quad (10)$$

We insert the form (5) in the free energy functional (2), and integrate over one period to obtain the following interfacial free energy

$$F = 2 \int_0^\infty dy \left(f_b - \frac{1}{4} \phi_q^2 q_x^2 (1 + u'^2) + \frac{1}{4} \phi_q^2 q_x^4 (1 + u'^2)^2 + \frac{1}{4} \phi_q^2 q_x^2 u''^2 \right) \quad (11)$$

where

$$\begin{aligned} f_b = & \frac{1}{4} (1 - \chi) \phi_0^2 + \frac{1}{8} (1 - \chi) \phi_q^2 \\ & + \frac{1}{2} \left(\phi_0^4 + \frac{3}{8} \phi_q^4 + 3 \phi_0^2 \phi_q^2 \right) \end{aligned} \quad (12)$$

is the bulk contribution. Writing the Euler-Lagrange equation for $w(y) \equiv u'(y)$ we obtain a non-linear second order differential equation

$$2w'' + 2w - 2q_x^2 (1 + w^2) 2w = 0 \quad (13)$$

which has the solution

$$w = w_\infty \tanh q_y y \quad (14)$$

with $w_\infty = -q_y/q_x = -\tan(\theta/2)$ as is required from the $y \rightarrow \pm\infty$ boundary conditions. We have thus found the order parameter profile.

$$\phi(x, y) = \phi_0 + \phi_q \cos[q_x x - \log(2 \cosh(q_y y))] \quad (15)$$

In order to calculate the grain-boundary energy, one substitutes (15) into the interfacial energy (11), and subtracts the bulk contribution f_b .

Using the analogy from the calculus of variation of a particle moving in a potential, we obtain

$$\gamma = 2 \int_0^\infty dy \left(\frac{dw}{dy} \right)^2 \frac{1}{2} \phi_q^2 q_x^2 \quad (16)$$

which reduces to

$$\gamma = \phi_q^2 q_x^2 \int_0^{w_\infty} \left(\frac{dw}{dy} \right) dw \quad (17)$$

and finally with the aid of $w_\infty = -q_y/q_x$ to

$$\gamma = \frac{2}{3} \phi_q^2 q_y^3 \sim \sin^3(\theta/2) \quad (18)$$

The order parameter we now have describes the chevrons very well. The tips of the V-shape structure are rounded-off, and far away from the interface the bulk phase is restored. The values of the grain-boundary energy are close to those obtained from full numerical minimization of the free energy functional (2), see [2]. The expression (18) for the grain boundary energy shows a θ^3 asymptotic scaling for small angles, a scaling which is easily understood. As the angle between grains, $\theta \rightarrow 0$, the grain boundary, and its energy, vanishes just as an interface between two coexisting phases vanishes as a control parameter $t \rightarrow 0$. Indeed as analyticity requires that $t \propto \theta^2$, one sees that the θ^3 behavior of the grain-boundary tension is just the same as the $t^{3/2}$ behavior of a surface tension obtained from mean-field theory. [16].

As $q_y \propto \theta$ for small angles, the width $u(y)$ scales as $1/q_y$, and the width w of the order parameter profile shows a $w \sim 1/\theta$ dependence, in accord with well established results [14].

The deficiency of the above approach is that it does not give the cross-over from the chevron to the omega morphology. For this end another approach will be used in the next section.

IV. DESCRIBING THE OMEGAS

In the bulk, the profiles of Eq. (4) minimize the free energy (2). In the grain boundary geometry they do not because the sharp tips at which they meet require too much conformational energy. The lamellae must somehow meet smoothly. The approach we employ in this section is to use the bulk-phase solution as a zero'th order approximation and determine a correction to it; that is, we write

$$\phi(x, y) = \phi_L(x, y) + \delta\phi(x, y) \quad (19)$$

After substitution of this form into Eq. (2) the free energy can be written as a sum of two parts:

$$F = F_L + \Delta F \quad (20)$$

where $F_L = F(\phi_L)$ is the bulk free energy. The excess free energy ΔF is the correction, which to second order in $\delta\phi$ is

$$\begin{aligned} \Delta F = & \left((1 - \chi) \phi_L + \frac{1}{3} \phi_L^3 \right) \delta\phi + \frac{1}{2} (1 - \chi + \phi_L^2) \delta\phi^2 + \nabla^2 \phi_L \nabla^2 \delta\phi + \\ & + \frac{1}{2} (\nabla^2 \delta\phi)^2 - \nabla \phi_L \nabla \delta\phi - \frac{1}{2} (\nabla \delta\phi)^2 \end{aligned} \quad (21)$$

Since ϕ_L minimizes F_L , we need to find the function $\delta\phi(x, y)$ that minimizes ΔF . This, in principle, is done via the Euler-Lagrange equation.

The boundary conditions for $\phi(x, y)$ follows from the symmetry of the grain boundaries, and from the requirement that ϕ approach its bulk value away from the interface:

$$\left. \frac{\partial \phi^n}{\partial^n y} \right|_{y=0} = 0 \quad (22)$$

$$\lim_{y \rightarrow \infty} \phi \longrightarrow \phi_L \quad (23)$$

In the above, n is odd. These conditions impose boundary conditions on $\delta\phi$, because ϕ_L is known, and $\phi = \phi_L + \delta\phi$.

The distortion field $\delta\phi(x, y)$ will be found based on an ansatz. Let us evaluate the y -derivative of the bulk tilted lamellar phase:

$$\left. \frac{\partial \phi_L}{\partial y} \right|_{y=0} = -q_y \phi_q \sin(q_x x) \quad (24)$$

It is reasonable, therefore, to assume that $\delta\phi$ has the following form:

$$\delta\phi(x, y) = f(y) \sin(q_x x) \quad (25)$$

The procedure we adopt is as follows. This ansatz for $\delta\phi$ is inserted into the free energy density. The system is periodic in the x direction, so the free energy can be integrated over one period. A grain-boundary energy functional which depends on the unknown amplitude $f(y)$ is obtained. This is minimized by an Euler-Lagrange equation, which results in a fourth order ordinary differential equation for $f(y)$. The boundary conditions Eqs. (22)-(23) will translate into boundary conditions on $f(y)$. The solution of the Euler-Lagrange equation gives, in principle, everything we want to know about the system: spatial distribution of the order parameter, line tension, etc.

We begin by putting our ansatz (25) into the expression (21) for ΔF . Integration over one period yields

$$\begin{aligned} \Delta F = & -\frac{1}{2} \left[1 - \chi + \frac{1}{4} (\varphi_q^2 + 4\varphi_0^2) - q_x^2 + q_x^2 q^2 \right] \varphi_q f \sin q_y y \\ & + \frac{1}{4} \left[1 - \chi + \varphi_0^2 + \frac{1}{4} \varphi_q^2 (2 - \cos 2q_y y) + q_x^4 - q_x^2 \right] f^2 \\ & + \frac{1}{2} \varphi_q q_y f' \cos q_y y - \frac{1}{4} f'^2 + \frac{1}{2} q^2 \varphi_q f'' \sin q_y y \\ & - \frac{1}{2} q_x^2 f f'' + \frac{1}{4} (f'')^2 \end{aligned} \quad (26)$$

The Euler-Lagrange equation for the function $f(y)$ is obtained by minimizing (26)

$$[A + C \cos(2q_y y)] f + B f'' + f'''' = 0 \quad (27)$$

where A, B and C depend on the parameters of the problem as follows:

$$\begin{aligned} A &= 1 - \chi + \varphi_0^2 + \frac{1}{2} \varphi_q^2 + q_x^4 - q_x^2 \\ B &= 2q_y^2 \\ C &= -\frac{1}{4} \varphi_q^2. \end{aligned}$$

This equation is similar to the Mathieu equation, which is the Schrödinger equation for an electron in a periodic (sinusoidal) one dimensional potential as appears in many solid state physics problems. The parameter A plays the role of the electron total energy, and C is the amplitude of the periodic potential. Unlike the solid-state case the periodicity here depends on θ , and therefore the boundaries of the Brillouin zone depend on the energy. Further, the coefficient B in front of “the kinetic energy” term in the Schrödinger equation language depends on the energy. Lastly, the differential equation is of fourth, not second order. Another useful observation is that equation (27) is invariant with respect to the spatial variable transformation $y \rightarrow -y$. Therefore, the solutions can be classified as symmetric and asymmetric. As we will see, the symmetric and asymmetric solutions do not satisfy separately the boundary conditions, so a combination of them will be needed.

Since this equation is linear with periodic coefficients, a solution to it will have the Bloch form. This is also known as the Floquet theorem [17]:

$$f(y) = e^{ky} g(y) \quad (28)$$

where $g(y)$ is a periodic function with period $d_y = 2\pi/2q_y$. Hence it is appropriate to write it as a Fourier series:

$$g(y) = \sum_{n=-\infty}^{\infty} a_n e^{inQy} \quad (29)$$

where $Q \equiv 2q_y$. Substituting the Bloch form Eq. (28) into Eq. (27), we get a sum of exponential terms. Demanding that the coefficients in front of every exponent vanish, we obtain the following recursion relation:

$$(A + B(k + inQ)^2 + (k + inQ)^4) a_n + \frac{1}{2} C(a_{n-1} + a_{n+1}) = 0 \quad (30)$$

The appearance of a_{n-1} and a_{n+1} is due to the $\cos(2q_y y)$ term in (27). At first glance, it seems that for every k , choosing “initial values” for the coefficients a_n ’s gives a valid solution. However, a closer inspection shows that for an arbitrary k vector the series a_n will diverge. Only a very specific value of k will give a convergent series.

The method by which we find this value is as follows (e.g., see Ref. [17]). Rewrite the recursion relations (30) as

$$\frac{a_n}{a_{n-1}} = \frac{-\frac{1}{2}C}{A + B(k + inQ)^2 + (k + inQ)^4 + \frac{1}{2}Ca_{n+1}/a_n} \quad (31)$$

for $n > 0$, and similarly

$$\frac{a_n}{a_{n+1}} = \frac{-\frac{1}{2}C}{A + B(k + inQ)^2 + (k + inQ)^4 + \frac{1}{2}Ca_{n-1}/a_n} \quad (32)$$

for $n < 0$. For very large values of n , a_{n+1}/a_n should be much smaller than one, so one can start from some $N \gg 1$, assuming that $a_{N+1}/a_N \rightarrow 0$, and get

$$\frac{a_N}{a_{N-1}} \approx \frac{-\frac{1}{2}C}{A + B(k + iNQ)^2 + (k + iNQ)^4} \quad (33)$$

then going *backward* gives the ratios $\{a_n/a_{n-1}\}$ for $0 < n \leq N$. Carrying out the same procedure for negative n 's one arrives at the *stopping condition*:

$$A + Bk^2 + k^4 = -\frac{1}{2}C \left(\frac{a_{-1}}{a_0} + \frac{a_1}{a_0} \right) \quad (34)$$

from which k is deduced, because the ratios a_1/a_0 and a_{-1}/a_0 are already known from Eqs. (31)-(32). The iteration scheme is to choose an initial guess for k , put it in (33), and use (31) and (32) successively for all $n \neq 0$. When $n = 0$ is reached, k is calculated from (34), and put back in (33). The process repeats until convergence is achieved. From the required boundary conditions at infinity, only k 's such that $\text{Re}(k) < 0$ are acceptable, recalling that the Bloch form (28) has e^{ky} .

It can be seen from (31), (32) that if a certain value of k gives a physical converging solution, then the complex conjugate of k , k^* , will also be a convergent solution, but with amplitudes a_{-n}^* . Solutions with $-k$ and $-k^*$ are possible, too, but are discarded because for them $f(y)$ diverges as $y \rightarrow \infty$. The functions with definite symmetry include both k and $-k$ and hence diverge at infinity. Consequently, by dropping the $-k$ solution we choose a specific combination of the symmetric and asymmetric functions with respect to y . The function f is a combination of the two independent solutions, and since it is real, it must be equal to:

$$f(y) = e^{ky} \sum_{n=-\infty}^{\infty} a_n e^{inQy} + c.c. \quad (35)$$

A choice of k such that $\text{Re}(k) < 0$ ensures that the disturbance will decay away far enough from the interface, $y \rightarrow \pm\infty$. The use of a linearization scheme left us with a linear ordinary differential equation, losing the ability to impose all boundary conditions, and forcing us to use only the first and third derivatives of f , which by the use of Eqs. (3), (22) and (25) are

$$\left. \frac{\partial f}{\partial y} \right|_0 = q_y \varphi_q \quad (36)$$

$$\left. \frac{\partial^3 f}{\partial y^3} \right|_0 = -q_y^3 \varphi_q \quad (37)$$

Putting (35) in these last relations, we obtain two linear equations for the free parameter a_0 . There is no redundancy because a_0 is, in general, complex. Having found a_0 we have found the complete solution to the problem.

V. BAND-GAPS AND DEGENERACY

In the usual Schrödinger equation, one encounter energetic gaps in the energy spectrum. They occur whenever the k -vector crosses the edges of a Brillouin zone. It should be expected that similar phenomenon happens here, too. Indeed, in our case it will happen whenever

$$\text{Im}(k) = mq_y \quad (38)$$

for some integer m . For k fulfilling (38) there is a *degeneracy* in the two previously found solutions. It can be seen by noticing that if (38) holds, k and k^* differ by $2imq_y$. Therefore, the amplitudes a_n corresponding to k^* are the same as those a_{n-1} corresponding to k , and the two solutions are dependent. If m is even, the two solutions are real.

In these band gaps there is a *splitting* of the real part of k ; another *independent* k -vector appears whose imaginary part is the same, but which has a different real part. The two solutions constructed by the Bloch form (28) are obviously independent. It should be noted that the appearance of energy gaps is a *mathematical* artifact and it should not affect the physical results, such as the grain-boundary energy. It is due to our approximative linearization scheme, and is not expected to occur if non-linearity would have been included.

VI. RESULTS

Figure 2 shows contour plots of the order parameter profile $\phi(x, y)$. The gray level indicate the size of the order parameter: black regions corresponding to the maximum values of ϕ (rich in A polymer), while white to its minimum value (rich in B polymer). The interaction is set to $\chi = 1$. The chevron morphology is represented in the Fig. 2a with tilt angle $\theta = 20^\circ$. A smooth changeover between the two lamellar phases is observed. For large angles ($\theta = 130^\circ$), the omega structure takes over as is shown in Fig. 2b, with large protrusions of the lamellae at the interface. Evidently, for large angles the excessive packing frustration of the chevrons cost more energy than the omegas. Chevron and omega morphologies are also shown in Fig. 3 but with $\chi = 0.76$ much closer to its critical value of $3/4$. As one goes away from the $y = 0$ interface, undulations of ϕ are encountered. There are more of them as the order-to-disorder transition (ODT) is approached, and the omega structure is more evident.

Figures 4 and 5 show the same plots, but with the lines of interface enhanced. The regions in white, gray and black correspond to $\phi < -0.2$, $-0.2 \leq \phi < 0.2$, and $\phi > 0.2$, respectively. The gray marks the interface between the A and B rich regions. The equi- ϕ lines clearly show the form of the interface in the chevron and omega morphologies. Notice that as the ODT is approached ($\chi = 0.76$ in Fig. 5), there are more undulations apparent on top of the bulk lamellar phase. In the chevron regime, the A/B interfacial width remains almost uniform, while in the omega regime it varies close to the kink [9].

Results for the grain-boundary energy γ_{TB} are shown in Fig. 6. The χ parameter is arbitrarily fixed to be $\chi = 0.76$. We show the grain-boundary energy calculated analytically by means of the methods of Sec. III and which is valid for small θ , as well as that calculated in Sec. IV. The grain-boundary energy γ_{TB} is an increasing function of the angle θ . In the small angle regime the grain-boundary energy obtained in Sec. III scales as $\gamma \sim \theta^3$. This scaling is also satisfied (to a good approximation) by the solutions obtained in Sec. IV. To see this, the same data is plotted in a different fashion in Fig. 7. In 7a, $\gamma^{1/3}$ is plotted as function of θ , while in 7b the data is plotted on a log-log plot. From both parts of Fig. 7 we conclude that the solution obtained in Sec. IV gives a power law with exponent of 2.91. Accuracy of the leftmost point of the solid curve in Fig. 7b is doubtful, due to poor convergence of the numerical iteration scheme for very small θ . As the tilt angle grows, deviations from the θ^3 behavior become larger, and the omega morphology, with its lower energy, appears gradually. For intermediate and large angles, our results are supported by a full numerical solution of this problem [2]. Presumably, for small angles there is agreement too (Netz, Andelman and Schick did not calculate surface tensions for very small angles). Note that in contrast to the full numerical solution in which the order parameter profile was obtained via a functional minimization, here we employed numerical means only to obtain the value of the eigenvalue k , while the profile equation was solved analytically. Our results agree well with experiment with the exception that we do not obtain the symmetry-breaking transition of the omega morphology [9]. To do so, one must add to an ansatz for the order parameter at least a term which varies as $2q_x x$, in addition to the fundamental term varying as $q_x x$. In Fig. 8 we show the k -vectors found by the use of the iteration scheme, as a function of tilt angle θ , with $\chi = 1$ fixed. Outside of the band-gaps, k and k^* are valid solutions, so for clarity only the k with $\text{Im}(k) > 0$ is shown. Notice that $\text{Re}(k)$ is always negative. The band-gaps are clearly seen on this graph as regions where $\text{Re}(k)$ have two distinct values. A check on the imaginary part of k in these regions reveals that it is an integer multiple of q_y .

VII. CONCLUDING REMARKS

We have used a simple Ginzburg-Landau free energy functional to investigate the profiles between lamellar phases of diblock copolymer. Our analytic results give good qualitative agreement with experiment in the weak segregation regime, and with full numerical solution of the same free energy model. The observed chevron morphology develops gradually into an omega morphology for intermediate tilt angles. For small angles, the use of a periodic order parameter with constant amplitude but varying wavevector suffices to describe the order parameter profile. This is

well described by the chevron morphology. For intermediate angles the change of the profile at the interface deviates significantly from the bulk, and requires a different treatment. The deviation from the bulk lamellae was found, and gave rise to the protrusion characterizing the omega morphology. The symmetry breaking of this phase was not obtained.

We were able to calculate grain-boundary energies and to determine that they scale as the cube of the angle [2,14] for small angles. As the tilt angle grows into the intermediate regime (the continuous chevron-to-omega transition), the energy deviates from this form. As $\theta \rightarrow 180^\circ$, the energy must go to zero. This does not occur in our analytic derivation, since then the linearization assumption is no longer valid.

Interesting extensions of the present work would describe interfaces of two perpendicular lamellar phases (so-called *T-junctions*), interfaces between modulated phases of other symmetries, and the inclusion of a twist instead of a tilt.

ACKNOWLEDGMENTS

We benefited from discussions with P. Rosenau and M. Schwartz. Partial support from the Israel Science Foundation founded by the Israel Academy of Sciences and Humanities — centers of Excellence Program, the U.S.-Israel Binational Foundation (B.S.F.) under grant No. 94-00291 and the National Science Foundation under Grant No. DMR 9876864 is gratefully acknowledged.

- [1] M. Seul and D. Andelman, *Science* **267**, 476 (1995).
- [2] R.R. Netz, D. Andelman, and M. Schick, *Phys. Rev. Lett.* **79**, 1058 (1997).
- [3] (a) S.P. Gido, J. Gunther, E.L. Thomas, and D. Hoffman, *Macromolecules* **26**, 4506 (1993); (b) S.P. Gido and E.L. Thomas, *Macromolecules* **27**, 6137 (1994).
- [4] Y. Nishikawa *et al.*, *Acta Polym.* **44**, 192 (1993); T. Hashimoto, S. Koizumi, and H. Hasegawa, *Macromolecules* **27**, 1562 (1994).
- [5] L. Leibler, *Macromolecules* **13**, 1602 (1980).
- [6] G.H. Fredrickson and E. Helfand, *J. Chem. Phys.* **87**, 697 (1987).
- [7] M. W. Matsen and F. Bates, *Macromolecules* **29**, 7641 (1996).
- [8] S. Villain-Guillot, Roland R. Netz, D. Andelman and M. Schick, *Physica A* **249**, 285-292 (1998).
- [9] M. W. Matsen, *J. Chem. Phys.* **107**, (19) (1997).
- [10] G. Gompper and M. Schick, *Phys. Rev. Lett.* **65**, 1116 (1990).
- [11] D. Andelman, F. Brochard, and J.-F. Joanny, *J. Chem. Phys.* **86**, 3673 (1987).
- [12] T. Garel and S. Doniach, *Phys. Rev. B* **26**, 325 (1982).
- [13] R. J. Spontak *et al.*, *Macromolecules* **29**, 4494 (1996).
- [14] P. G. de Gennes and J. Prost, *The Physics of Liquid Crystals*, 2nd ed. (Clarendon, Oxford, 1993), p. 484.
- [15] A. C. Newell, T. Passot, C. Bowman, N. Ercolani, R. Indik, *Physica D* **97**, 185-205 (1996).
- [16] J. S. Rowlinson and B. Widom, *Molecular Theory of Capillarity* (Oxford University Press, New York, 1982).
- [17] P. M. Morse and H. Feshbach, *Methods of Theoretical Physics* (McGraw-Hill, New York, 1953), p. 557-558.

- **Fig. 1:** A schematic drawing of the geometry of the system. In (a) the tilt angle θ between the normal of the two lamellar phases is shown. The bulk periodicity d is smaller than the local periodicity d_x at the interface, $y = 0$. In (b) a schematic drawing of a chevron morphology with rounded V-shaped tips is shown.
- **Fig. 2:** Black and white contour plot of the order parameter profile, as obtained from the profile solutions of Sec. IV. The grayness denotes the value of the order parameter (A/B relative concentration). Black domains are A-rich, white domains are B-rich. The value of the interaction parameter is $\chi = 1$ and the average concentration is $\phi_0 = 0$. For the small angle ($\theta = 20^\circ$, top plot) chevron morphology appears, while for $\theta = 130^\circ$ (bottom plot) omega takes over.
- **Fig. 3:** Same as Fig. 2, but with $\chi = 0.76$. Top plot is for $\theta = 20^\circ$ and the bottom plot is for $\theta = 130^\circ$. The system is closer to the ODT than that of Fig. 2, and the modulation of the lamellae are more prominent.
- **Fig. 4:** Black and white contour plot, with line enhancement. Black regions are A-rich ($\phi > 0.2$), white regions are B-rich ($\phi < 0.2$), while gray regions marks the interfacial region ($-0.2 \leq \phi \leq 0.2$). Top plot is for $\theta = 20^\circ$ and in the bottom plot $\theta = 130^\circ$. The interaction is set to $\chi = 1$.
- **Fig. 5:** As in Fig. 4, but with $\chi = 0.76$. Top plot is for $\theta = 20^\circ$ and the bottom plot is for $\theta = 130^\circ$. Comparison with Fig. 4 shows that for fixed tilt angle θ , the omega structure and the modulations of the bulk are more evident closer to the disordered phase.
- **Fig. 6:** Plot of the grain-boundary energy γ as function of the tilt angle θ , for $\chi = 0.76$. θ ranges from 0 to 180° . The curve marked with rectangles shows the results obtained in Sec. III for the chevron morphology, with $\gamma = \frac{2}{3}\phi_q^2 q_y^3$. The curve with circles shows the results of Sec. IV. Notice that the two expressions are very similar, but at some intermediate values of θ there is a crossover from the chevron to the omega morphology. Evidently, for large tilt angles the omegas cost less energy.
- **Fig. 7:** In (a) the grain-boundary energy γ of Fig. 6, is plotted as $\gamma^{1/3}$ against the tilt angle θ . The dashed curve with rectangles is straight for small angles, depicting perfect $\gamma \sim \theta^3$ dependence. The curve marked with circles shows a power exponent 2.91. In (b) the two line tension are plotted on a log-log plot. The results of Sec. III show θ^3 scaling, while the omegas show a smaller power exponent. The small errors in our numerical scheme to find the wavevector k are crucial for the leftmost points, and this may easily change the line tension exponent from the expected 3 to 2.91.
- **Fig. 8:** The imaginary and real parts of the wave-vector k in expression (28) are shown in (a), for $\chi = 1$. The line with rectangles corresponds to the imaginary part. Only the positive imaginary part is shown. The line with circles corresponds to the real part of k . Dotted line shows q_y , being the characteristic length scale in the y -direction. Notice the splitting of the real part of k in the band gaps. An enlargement of the same curve of the imaginary part of k , for $17^\circ \leq \theta \leq 50^\circ$ is shown in (b). The black lines indicates integer multiples of q_y . Three band gaps are shown, around 18° , 26° and 42° . In these gaps $\text{Im}(k) = imq_y$ for some integer m .

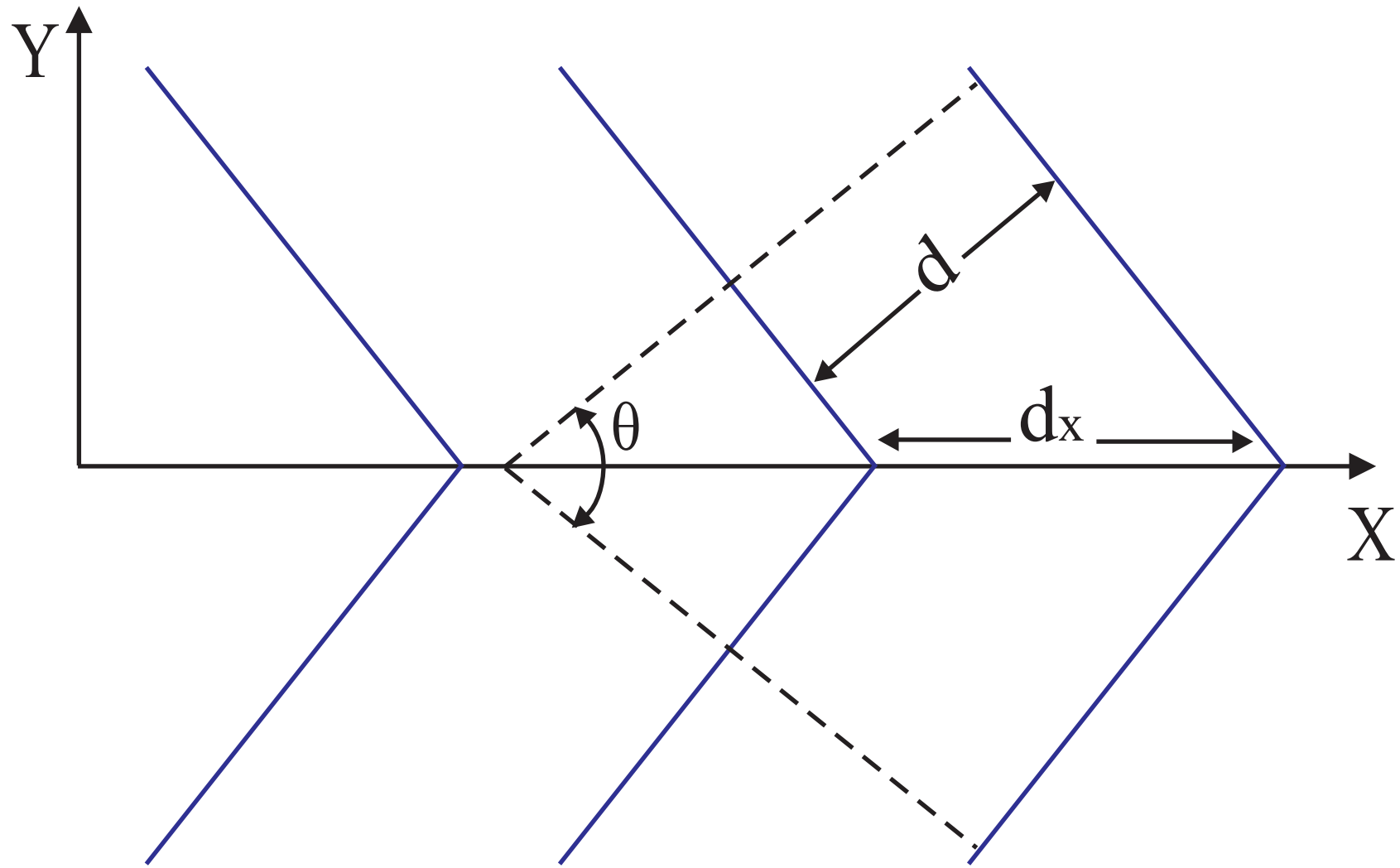


Fig. 1a

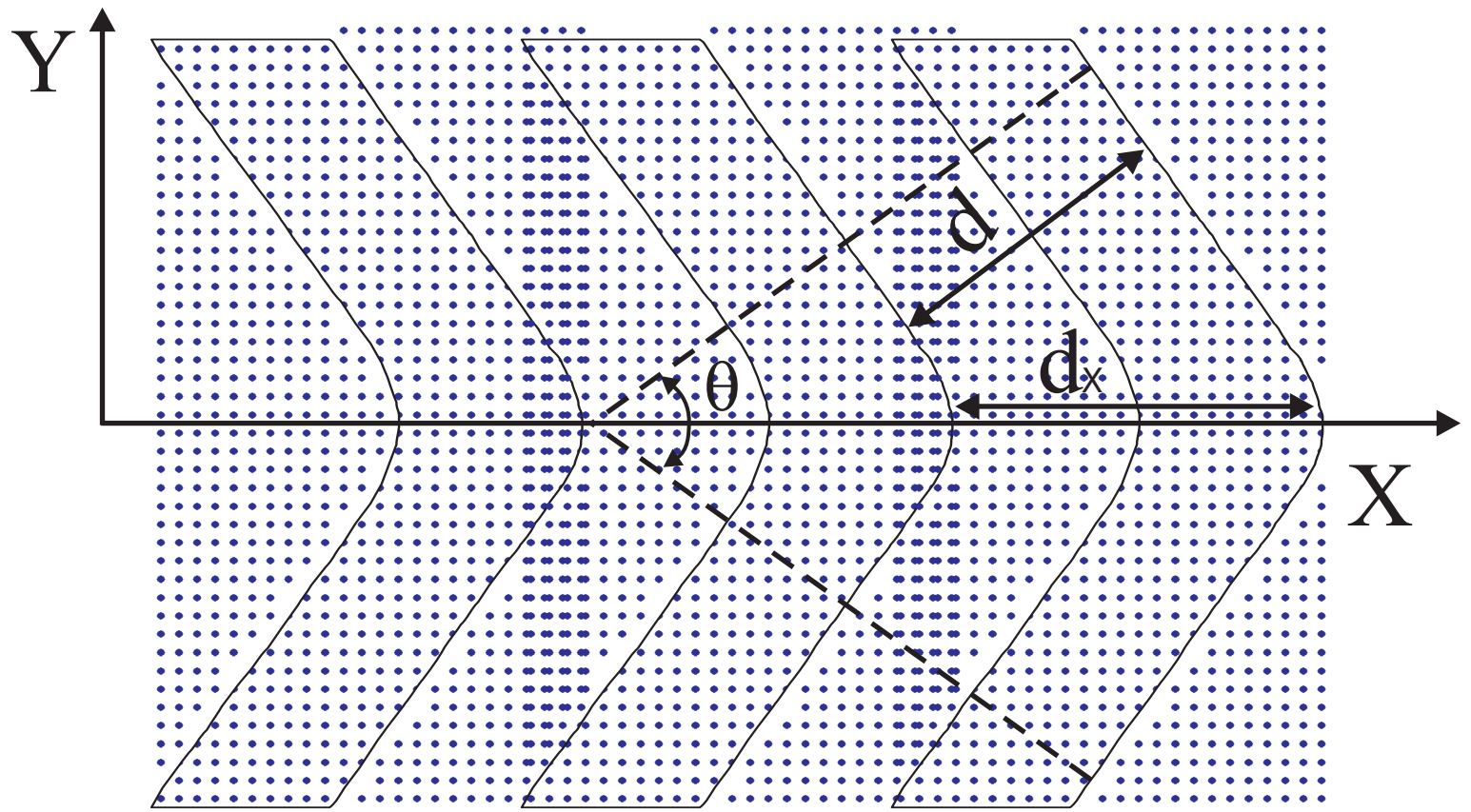


Fig. 1b

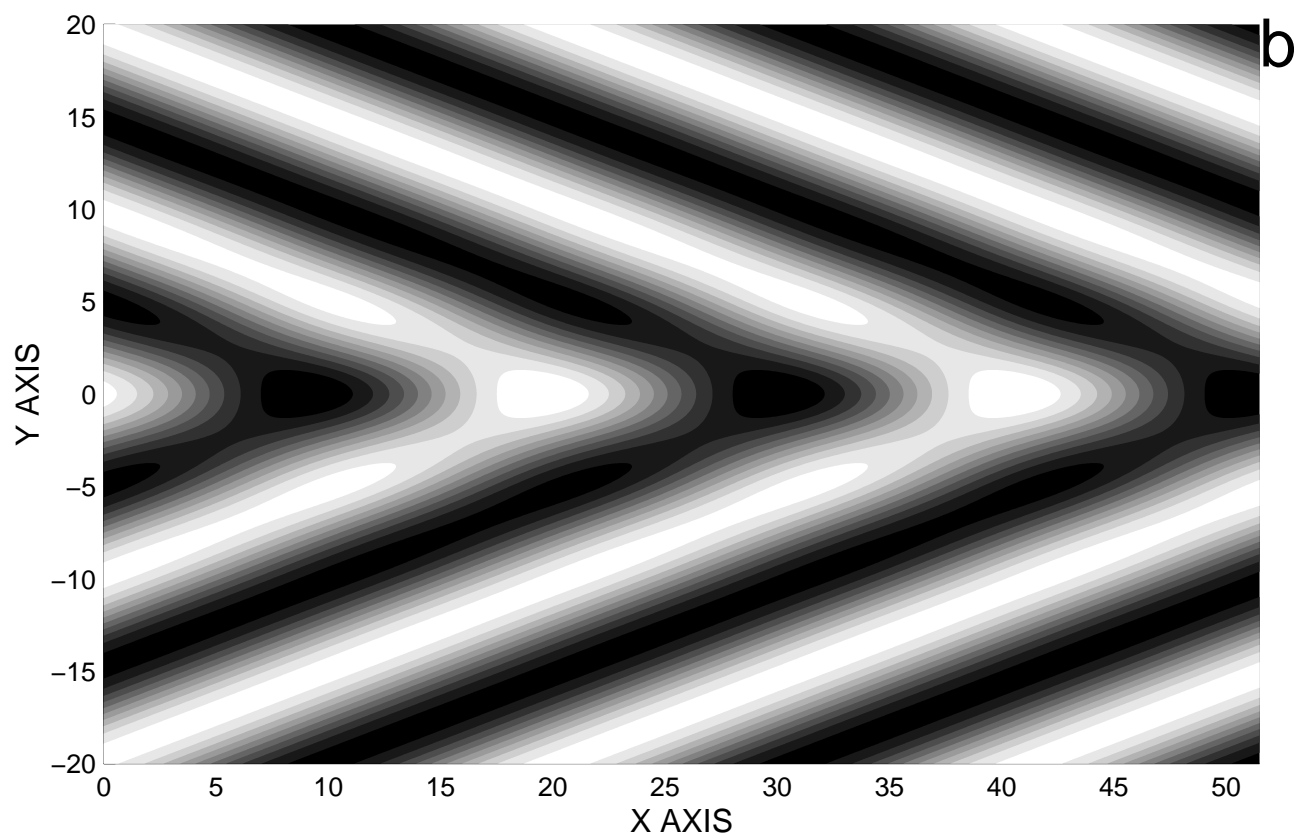
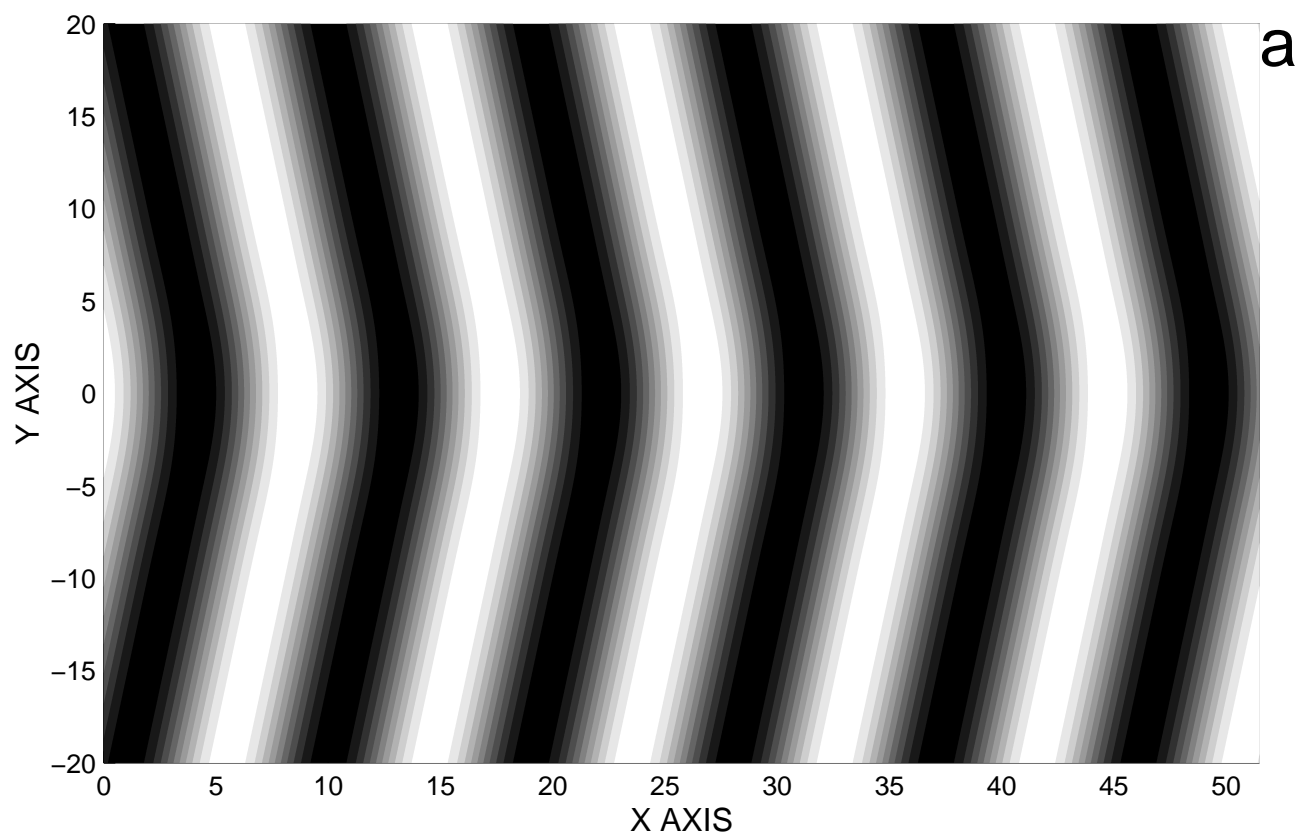


Fig. 2

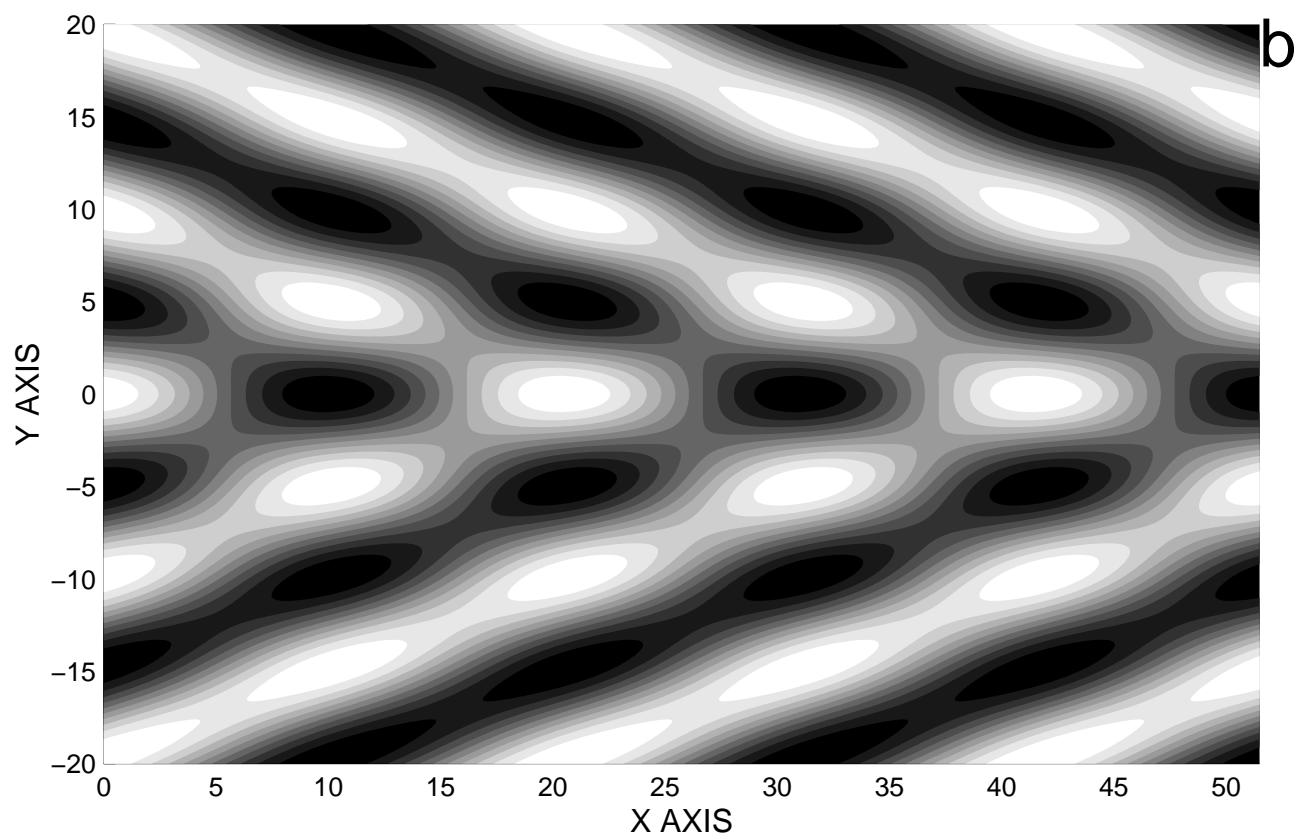
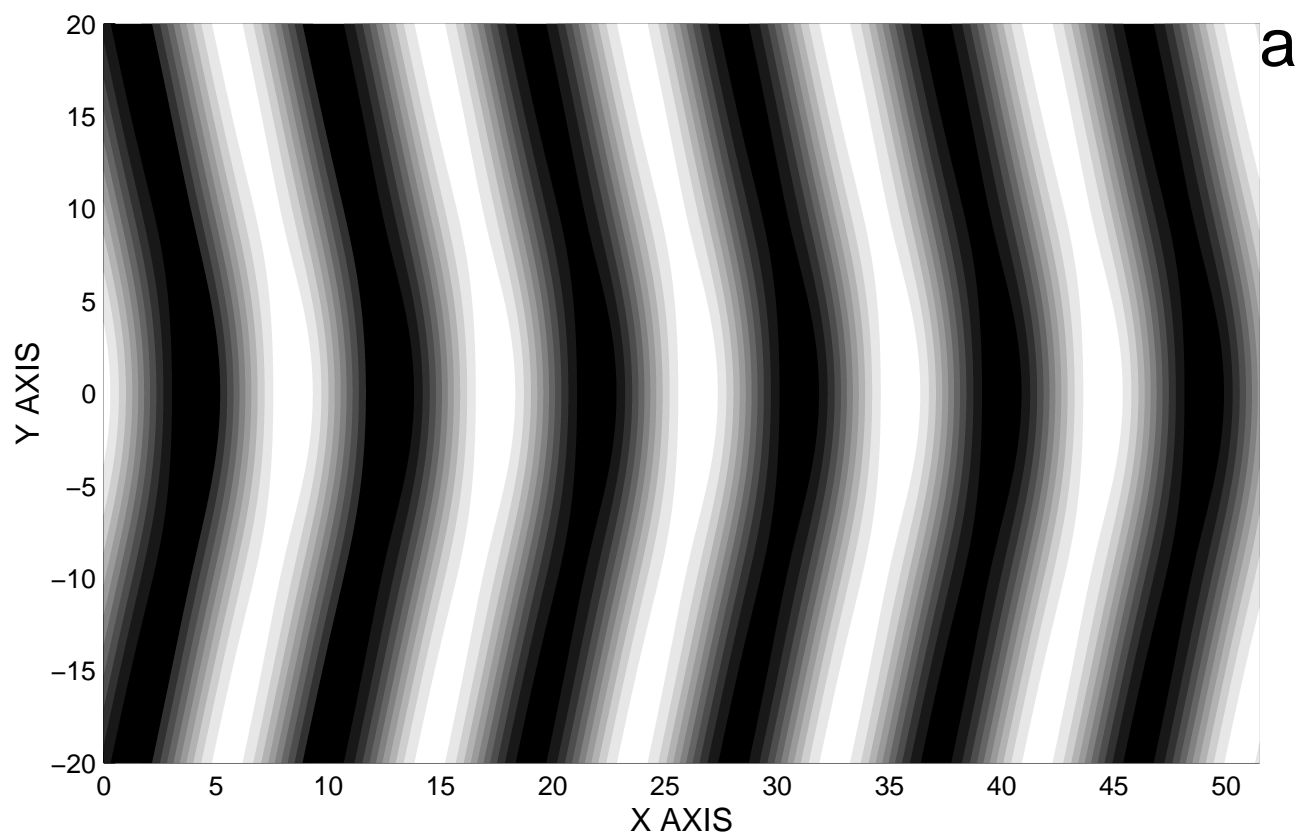


Fig. 3

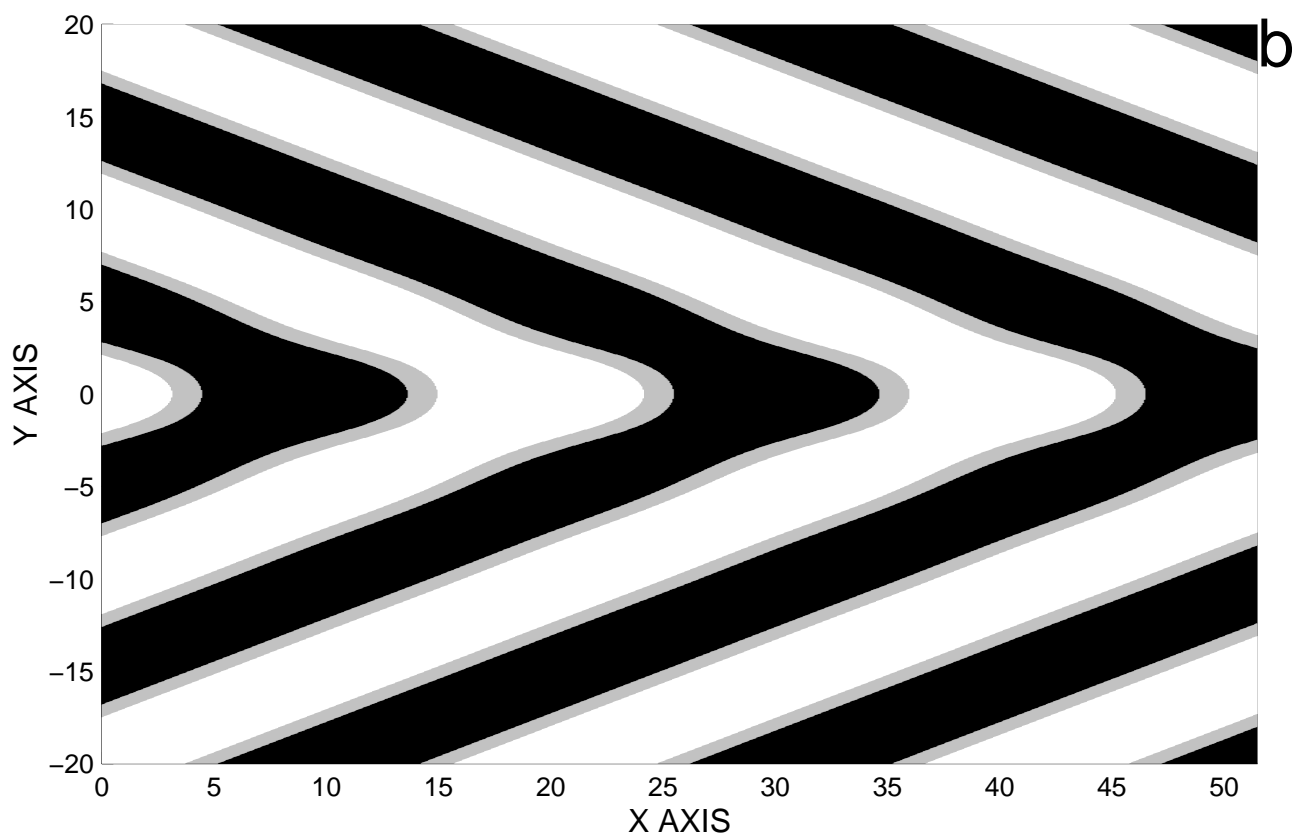
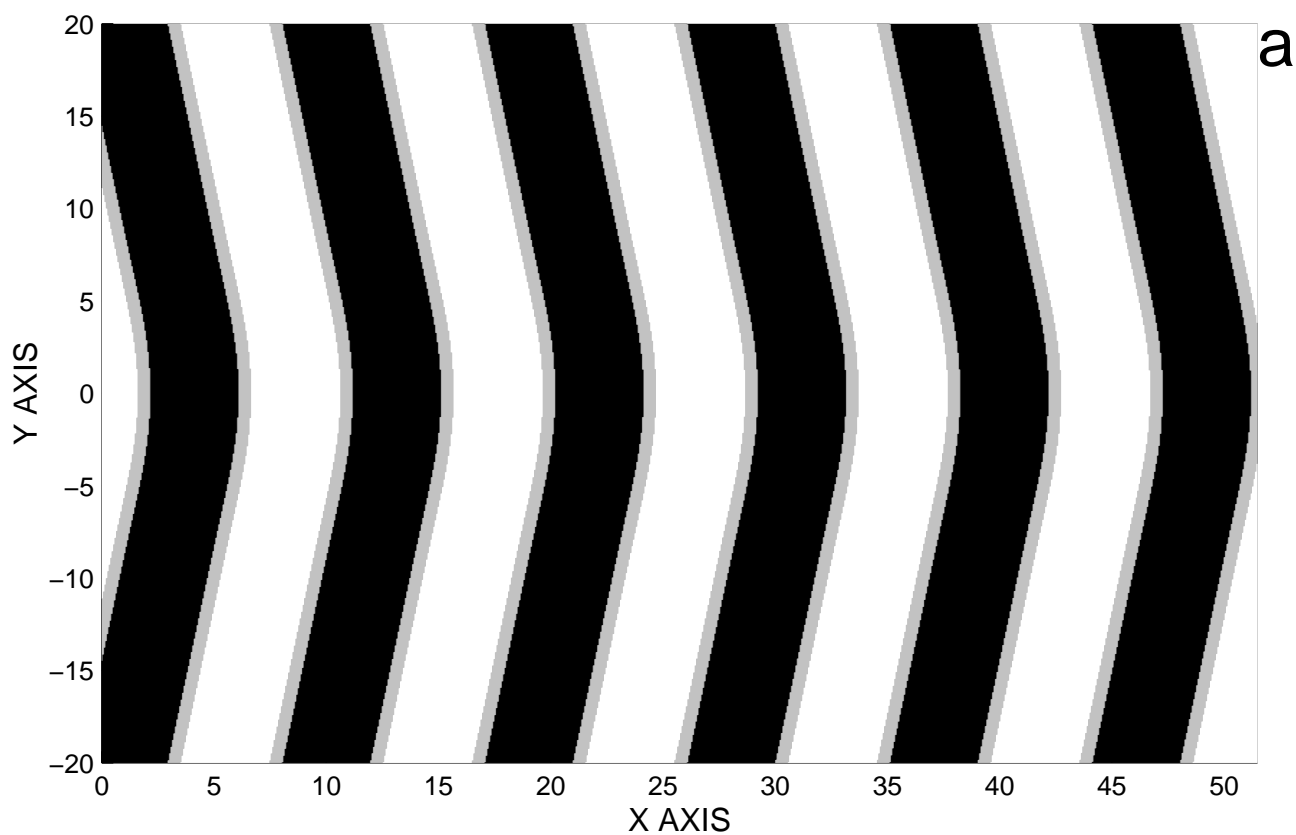


Fig. 4

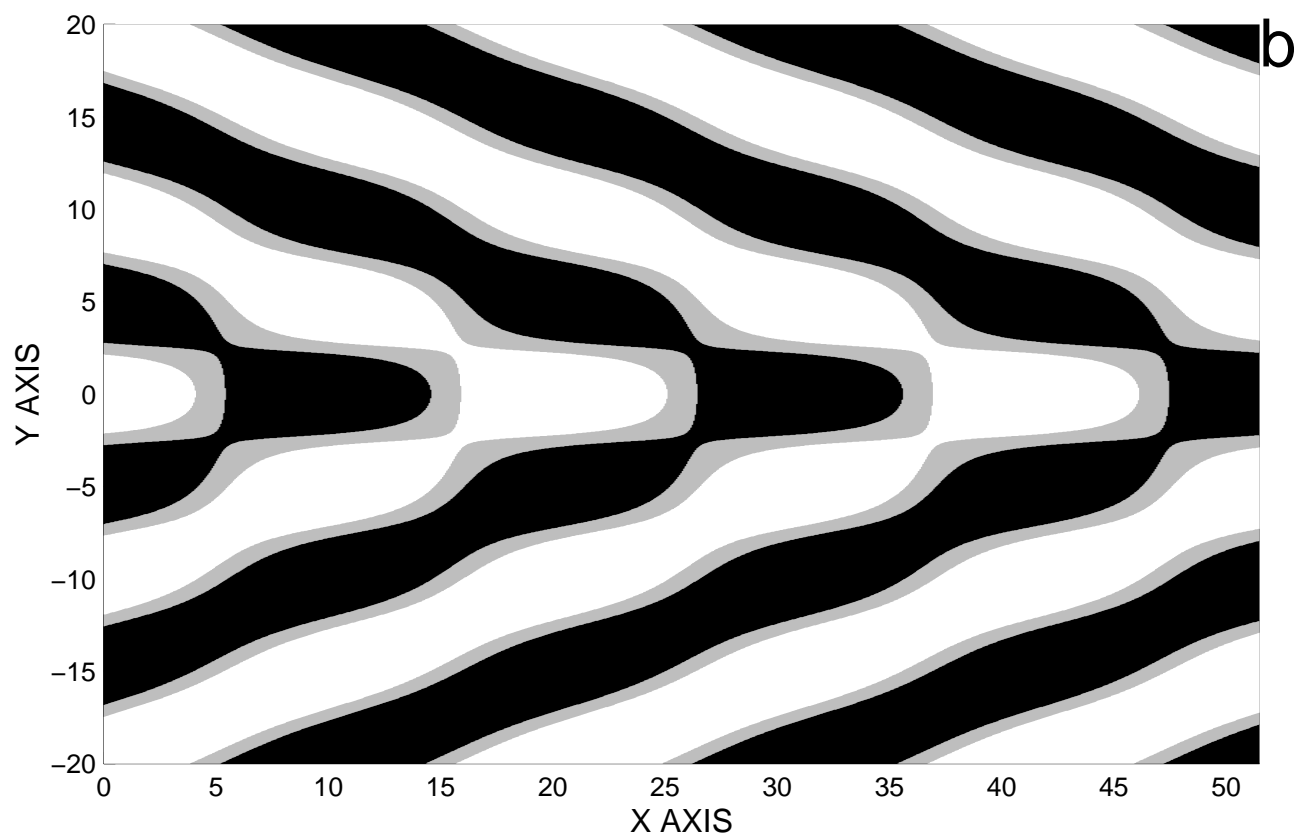
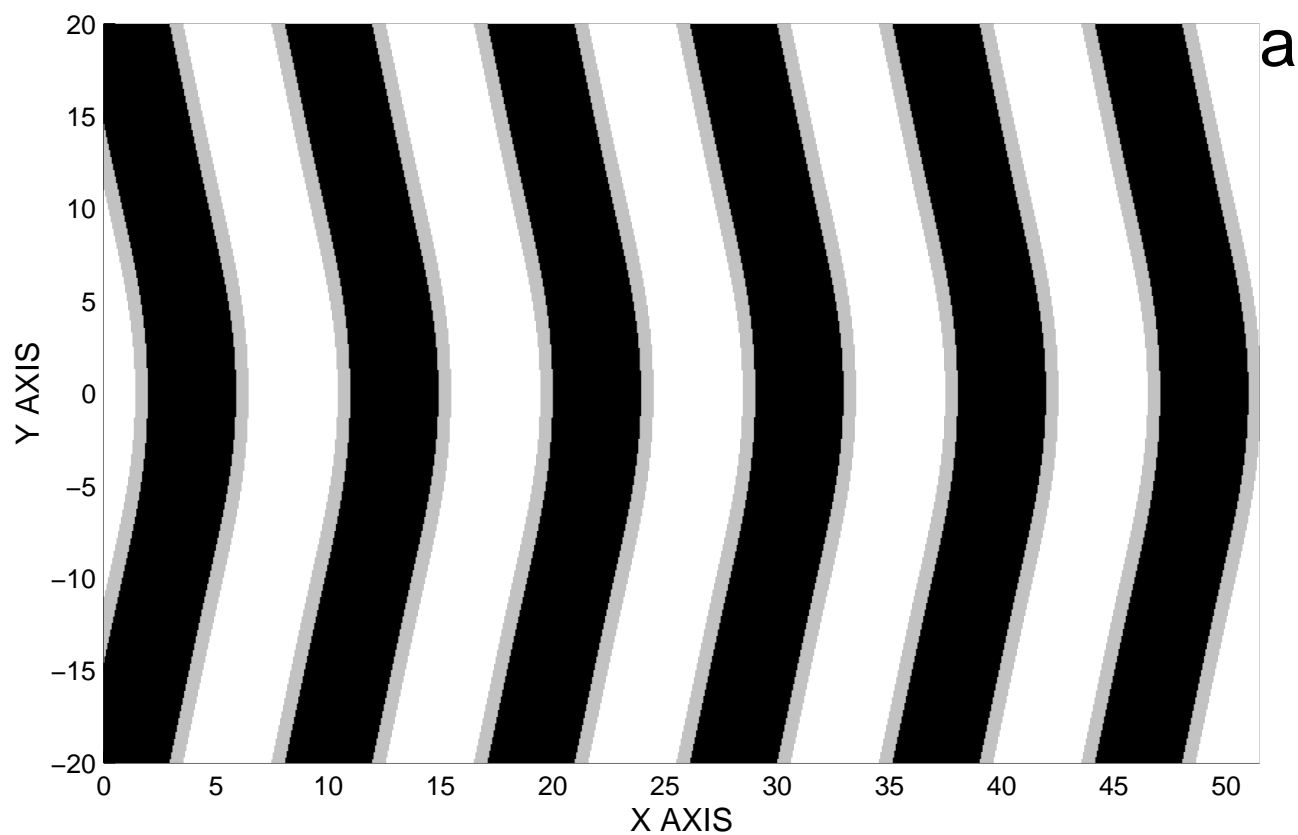


Fig. 5

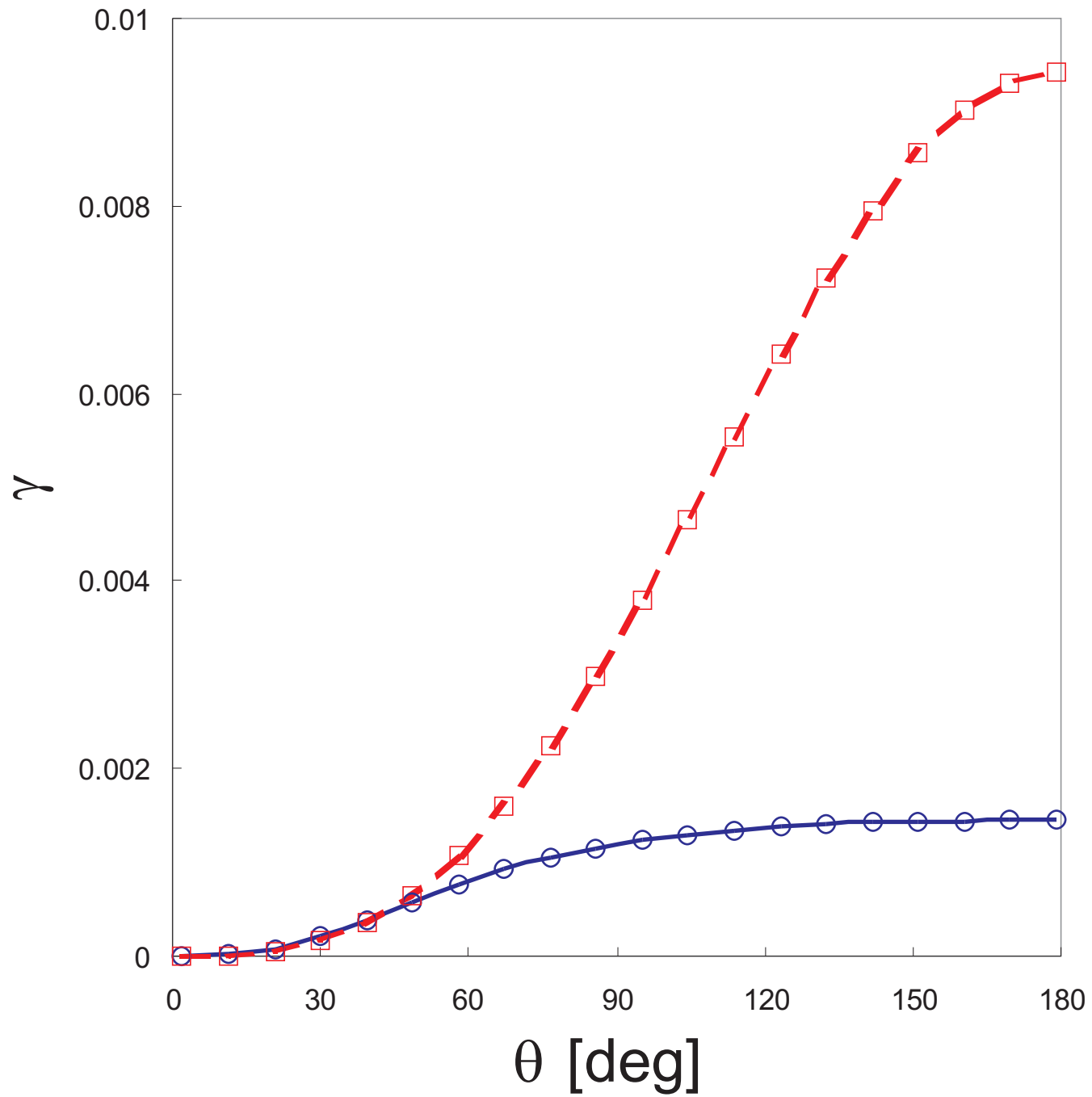


Fig. 6

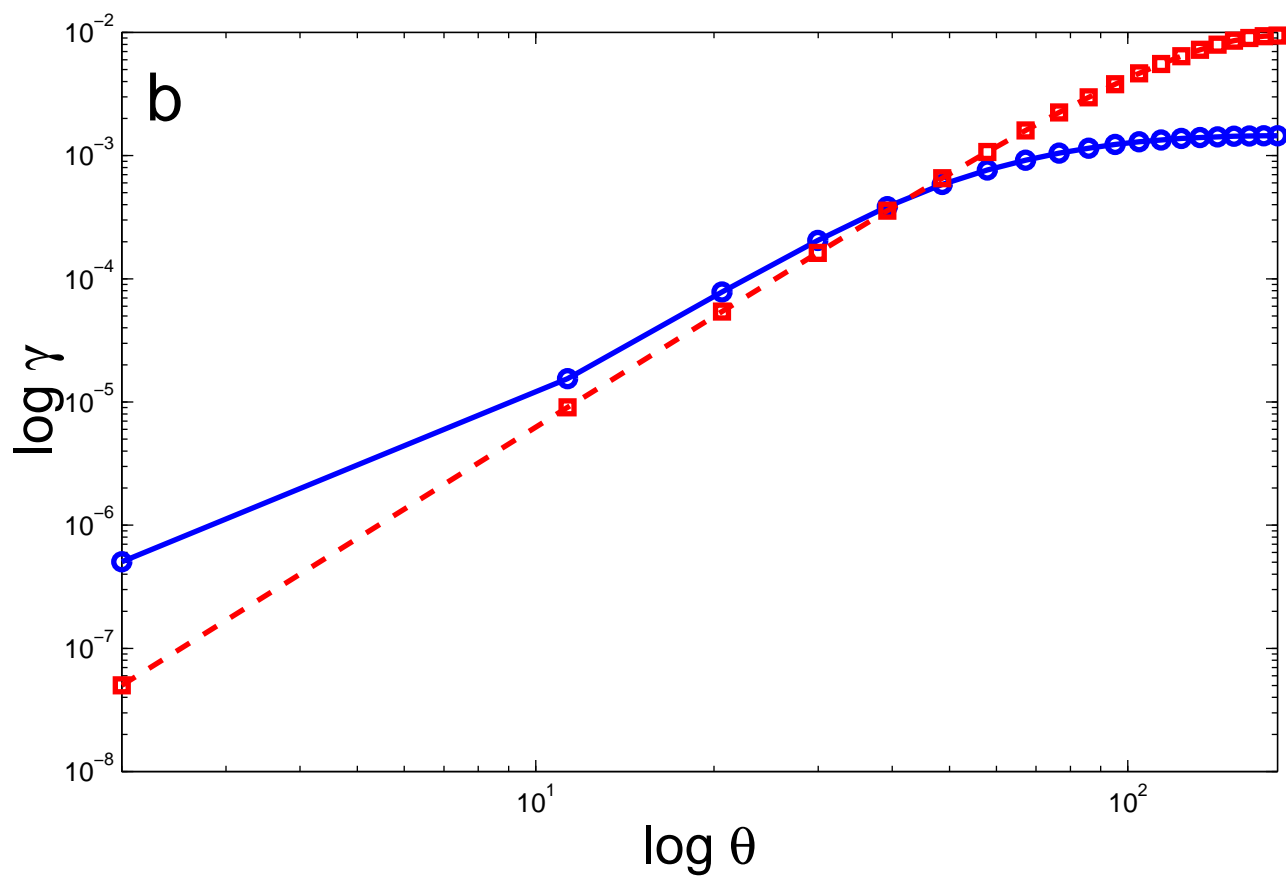
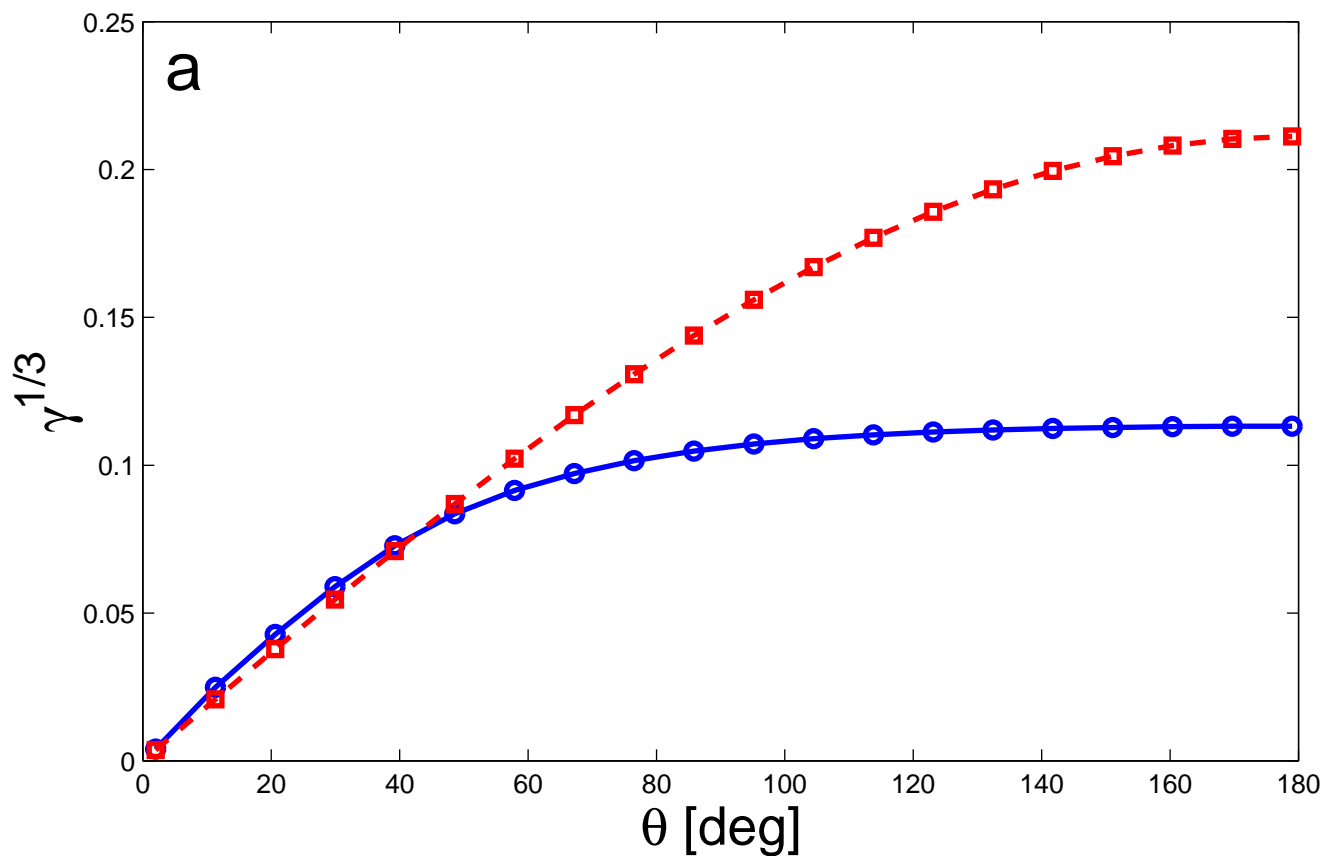


Fig. 7

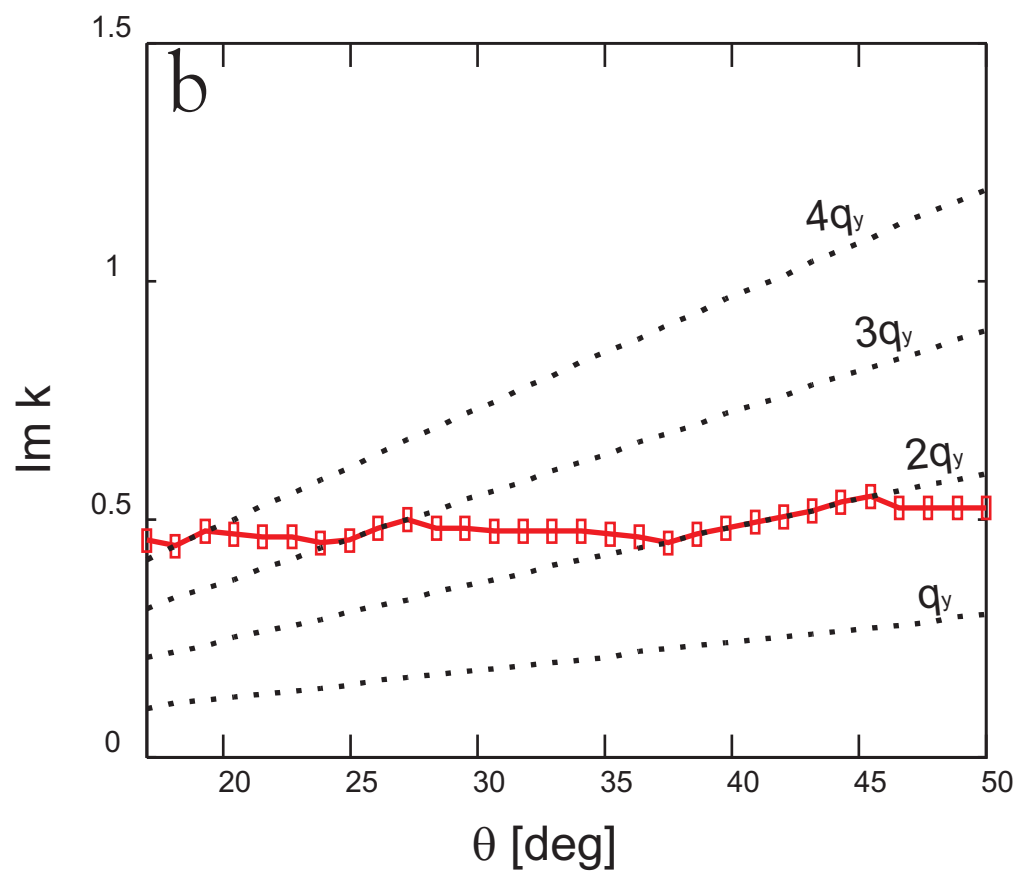
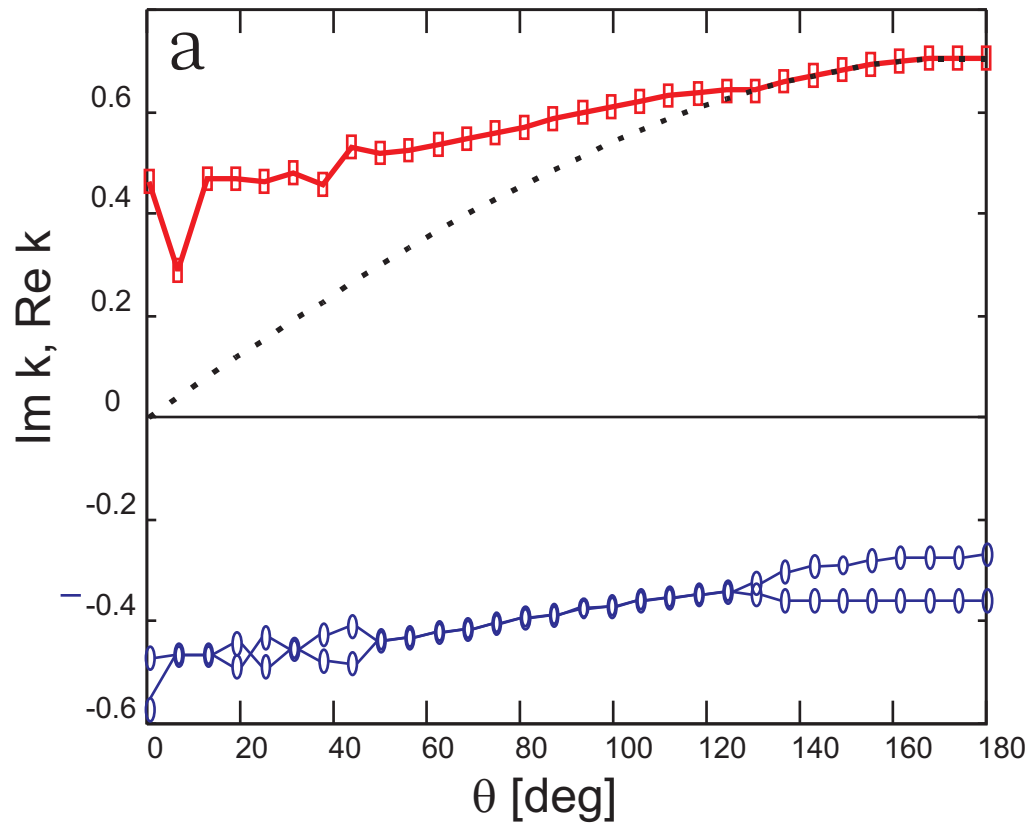


Fig. 8